Journal of Power Sources 375 (2018) 131–137

Contents lists available at ScienceDirect

Journal of Power Sources

journal homepage: www.elsevier.com/locate/jpowsour

Mechanistic elucidation of thermal runaway in potassium-ion batteries

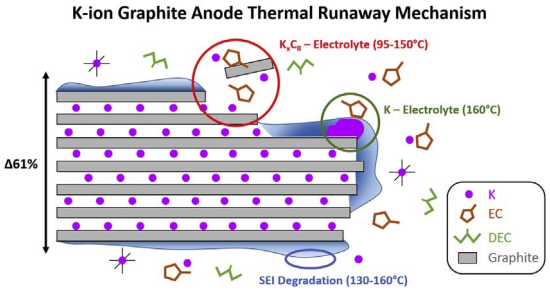
Ryan A. Adams, Arvind Varma, Vilas G. Pol*

Davidson School of Chemical Engineering, Purdue University, West Lafayette, IN 47907, United States

HIGHLIGHTS

- Thermal runaway from K-ion graphite anode initiates at 100 °C.
- 63% less total heat is generated for the K-ion system as compared to Li-ion.
- Consumption of all intercalated K occurs by 150 °C, fueling the peak at 100 °C.
- K-ion SEI manipulation can mitigate this by preventing graphite-electrolyte contact.

GRAPHICAL ABSTRACT



ARTICLE INFO

Keywords:
Potassium-ion batteries
Thermal runaway
Differential scanning calorimetry
Graphite anode

ABSTRACT

For the first time, thermal runaway of charged graphite anodes for K-ion batteries is investigated, using differential scanning calorimetry (DSC) to probe the exothermic degradation reactions. Investigated parameters such as state of charge, cycle number, surface area, and binder demonstrate strong influences on the DSC profiles. Thermal runaway initiates at 100 °C owing to K_xC_8 – electrolyte reactions, but the K-ion graphite anode evolves significantly less heat as compared to the analogous Li-ion system (395 J g^{-1} vs. 1048 J g^{-1}). The large volumetric expansion of graphite during potassiation cracks the SEI layer, enabling contact and reaction of KC_8 – electrolyte, which diminishes with cycle number due to continuous SEI growth. High surface area graphite decreases the total heat generation, owing to thermal stability of the K-ion SEI layer. These findings illustrate the dynamic nature of K-ion thermal runaway and its many contrasts with the Li-ion graphite system, permitting possible engineering solutions for safer batteries.

1. Introduction

Safety remains a primary concern of lithium ion batteries (LIBs) despite more than two decades of commercialization and widespread usage [1,2]. Thermal runaway can initiate from exothermic breakdown of the SEI layer on carbon anodes, which starts typically at 120 °C [3–5]. Heat generation from electrolyte breakdown and reaction with lithiated carbon leads to cathode decomposition and release of oxygen, increasing system pressure and reactivity [6–8]. By 200 °C, total exothermic heat generation of 2 kJ g^{-1} electrode material occurs, resulting in intense explosions and flames [9]. Evolution of CO_2, O_2, H_2, POF_3, and HF from decomposition reactions of electrolyte, salt, polymer binder, and electrodes contributes to increased heat and pressure, accelerating the process [10]. As the initiating process for thermal runaway of LIBs, the degradation reactions of SEI breakdown are of great interest to understand and mitigate [11]. Factors including state of charge (SOC), electrolyte composition, binder, and carbon material properties significantly impact thermal runaway [3]. Various strategies, including alternative binders, electrolyte components, and flame retardant additives, can mitigate heat generation in the Li-ion battery system, but typically adversely affect electrochemical performance [12,13]. In practice, LIBs must be carefully designed and regulated for

* Corresponding author.
E-mail address: vpol@purdue.edu (V.G. Pol).

https://doi.org/10.1016/j.jpowsour.2017.11.065
Received 20 October 2017; Received in revised form 10 November 2017; Accepted 21 November 2017
0378-7753/ © 2017 Elsevier B.V. All rights reserved.

safe operation, leading to manufacturing cost increases for failsafe mechanisms (gas relief valves, safety vents, etc.) and rigorous testing by heating, short-circuiting, overcharging, nail puncturing, and crushing of cells [9].

Recently, non-aqueous potassium-ion batteries (KIBs) have received interest as a novel energy storage technology, utilizing inexpensive and abundant potassium as the charge carrier ion. KIBs operate in a manner similar to LIBs, with K ion intercalation between cathode and anode through an organic solvent-inorganic salt electrolyte medium [14,15]. Despite its larger ionic size, KIBs have an advantage over its competitor, the sodium-ion battery, as K ions can electrochemically intercalate into graphite to form stage-one KC_8 structure for 279 mAh g^{-1}, whereas Na is limited to NaC_{64} for 35 mAh g^{-1} [16,17]. Formation of KC_8 causes 61% volumetric expansion of graphite however, resulting in electrode pulverization and excessive solid electrolyte interphase (SEI) formation over time [17,18]. Utilization of functionalized binders, such as sodium carboxymethylcellulose (CMCNa), and optimized electrolyte significantly improve electrochemical performance, with increased first cycle Coulombic efficiency and long-term cycling stability [19,20]. Many carbon materials have been evaluated for KIB anodes, including hard carbon microspheres, carbon nanofibers, F- or N-doped graphene, polynanocrystalline graphite, and tire-derived hard carbon [21–27]. The expanded graphitic interlattice spacing mitigates electrode pulverization induced by volumetric changes, resulting in exceptional rate capability and cycling stability. Several KIB cathode materials have shown promising performance, including layered K metal oxide materials, such as $K_{0.3}MnO_2$, $K_{0.7}Fe_{0.5}Mn_{0.5}O_2$, and $K_{0.6}CoO_2$, as well as vanadium phosphate $KVPO_4F$ and $KVOPO_4$ [28–31]. Despite this exceptional electrochemical performance, no prior studies have been reported regarding KIB carbon anode safety to evaluate the practicality of this novel battery system.

Possible safety concerns for KIBs arise from several aspects: (1) Potassium metal is dangerous due to its formation of highly reactive superoxide compounds. (2) K metal melts at 63.5 °C, as compared to 97.8 °C for Na and 180.5 °C for Li. (3) Stage-one KC_8 is pyrophoric. (4) An organic based electrolyte is utilized, making the system flammable and self-sustaining in exothermic breakdown reactions. While K metal anode is not utilized per se in the full cell, the possibility of K metal deposition and plating on the carbon anode remains. Additionally, properties of the K-ion SEI layer remain largely unknown, although some studies have predicted it to be more stable than Li-ion and Na-ion SEI with increased fraction of inorganic salts, such as K_2CO_3 [32–34]. In this study, graphite is the primary electrode material investigated, due to its favorable energy density, voltage plateau, and commercialization viability. Differential scanning calorimetry (DSC) is the primary technique used to study the KIB graphite system, with selective sample preparation to determine the thermal runaway mechanism and heat generation in comparison to LIBs. To our knowledge, this is the first study to explore safety aspects of KIBs, analyze thermal runaway of graphite anode, and evaluate its practicality for commercialization.

2. Experimental

Electrodes were prepared with a ratio of 80 wt. % active material (e.g. synthetic graphite), 10 wt. % conductive additive (Timcal Super C65), and 10 wt. % polymer binder (polyvinylidene fluoride). Using N-methyl-2-pyrrolidone as solvent, a slurry was mixed for 20 min and tape-cast onto aluminum foil via doctor-blade. For laminates constructed with functionalized binders, such as CMCNa or Na-alginate, water was utilized as solvent. The laminate was dried for 12 h in a vacuum oven set to 80 °C, and then 12 mm diameter electrodes were punched out with an active material density of ~2.5 mg cm^{-2}. Electrochemical tests were performed in a coin-type 2032 half-cell, using potassium metal as the counter and reference electrode. Whatman 934-AH glass microfiber was used as separator and 0.8 M KPF_6 in a 1:1 (by volume) mixture of ethylene carbonate (EC)/diethyl carbonate (DEC) was utilized as electrolyte. Galvanostatic cycling was performed with an Arbin cycler in a voltage range of 0.005–1.5 V at room temperature. To condition for differential scanning calorimetry (DSC) analysis, half-cells were cycled at C/10 current density (determined by theoretical capacity of 279 mAh g^{-1}, according to KC_8 stage-one structure) for 5 cycles for the base case, with the corresponding voltage set at equilibrium condition (< 1 μA current). To remove electrolyte, the electrode was washed with dimethyl carbonate (DMC) three times, with vacuum drying in-between. Lithium-ion coin cells were prepared using copper-foil cast graphite electrodes, with Li metal as the counter electrode, Celgard 2500 as separator, and 1 M $LiPF_6$ in 1:1 (by volume) EC/DEC.

DSC was performed with a TA Instruments Q20 instrument, at a scan rate of 5 °C min^{-1}. To perform DSC analysis, the conditioned coin cell was dissembled in an argon glovebox, with the potassiated electrode material scraped off the current collector into a hermetically sealed aluminum pan. A Mettler Toledo XS3DU microbalance was used to precisely measure mass loading of wetted electrode material, with an average 1–2 mg sample size. Low mass loading was used to prevent gassing and breakage of the hermetic seal at higher temperatures due to electrolyte evaporation, and results showing irregular jumps or weight loss after DSC measurements were removed. To ensure consistency of results, multiple coin cells were constructed for each trial, with 2 samples run from each individual electrode, and representative data is provided in this study. Scanning electron microscopy (FE-SEM) images were recorded using a Hitachi S-4800 microscope. Powder X-ray diffraction (XRD) was utilized to characterize the crystalline phase via the Bragg – Brentano method (Rigaku SmartLab X-ray diffractometer). A Cu-Kα X-ray source (λ = 0.154 184 nm) was used to obtain the XRD patterns (2θ = 5–80°) at a scanning rate of 2° min^{-1} with samples sealed by Kapton tape. Raman spectra were collected with a 633 nm laser utilizing a Thermo Scientific DXR Raman microscope and an inert sample holder loaded in an argon glovebox. Surface area analysis (Quantachrome Instruments NOVA 2200e) was conducted using nitrogen adsorption/desorption isotherm measurements at 77 K. Samples were degassed for 12 h at 300 °C prior to measurements. Multipoint specific surface area calculations were performed using the linear portion (P/P_0 = 0.05–0.30) of the Brunauer – Emmett – Teller (BET) model. Stage-one KC_8 was chemically synthesized by taking stoichiometric ratios of graphite and K metal, and heating in an inert atmosphere under stirring at 200 °C for 2 h. High surface area graphite was produced by ball milling (Quantachrome Instruments MillPrep-Micro Ball Mill) for either 1 or 5 h, followed by particle sieving (Endecotts > 25 μm & < 53 μm stainless steel sieve) to improve particle size homogeneity.

3. Results and discussion

A typical second cycle charge-discharge voltage profiles for a graphite anode tested in Li-ion and K-ion systems are shown in Fig. 1. At 20 mA g^{-1}, the graphite anode achieves close to the theoretical capacities of 279 mAh g^{-1} for KC_8 and 372 mAh g^{-1} for LiC_6. The higher intercalation potential of K versus Li reduces the risk of plating and dendrite formation on the anode, which can occur at very low potentials, high currents, and low operating temperatures [35]. The first cycle voltage profile is shown in Fig. S1a, where the K-ion system has a Coulombic efficiency of 43%, as compared to 80% for Li-ion, likely occurring due to excessive SEI formation from the 61% volume expansion during potassiation [17]. Extended galvanostatic cycling, as shown in Fig. S1b, reveals a capacity fade of 35% over 50 cycles for the K-ion graphite anode, due to electrode pulverization and SEI buildup as signified by 95% average Coulombic efficiency. In contrast, the Li-ion graphite anode shows rapid stabilization and 99.9% average Coulombic efficiency over 50 cycles. The synthetic graphite material properties are characterized in Fig. S2, with Raman spectrum, XRD pattern, SEM imaging, and N_2 sorption isotherms, giving a BET surface area

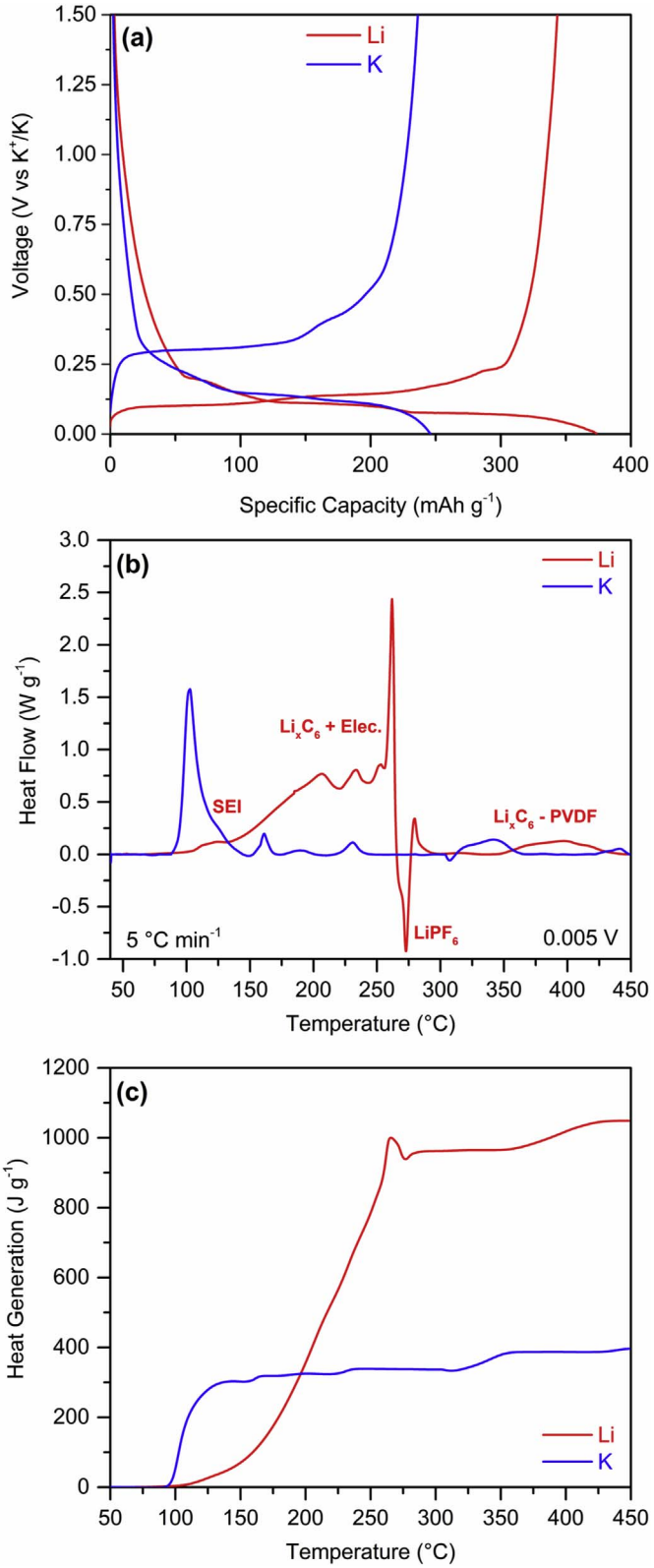


Fig. 1. (a) Typical charge-discharge voltage profile for graphite electrode in Li-ion and K-ion battery configuration at 20 mA g^{-1} current density. (b) DSC profiles of fully charged graphite electrodes prepared by a Li-ion or K-ion battery configuration, with Li-ion degradation reactions labeled. (c) Total heat generation as a function of temperature of DSC profiles.

3.4 m^2 g^{-1}. For these DSC studies, the electrodes with polyvinylidene fluoride (PVDF) binder were analyzed, to analyze the influence of the native K-ion SEI layer and volumetric changes on thermal runaway.

Fig. 1b presents typical DSC profiles for charged graphite anodes in Li-ion and K-ion batteries. The Li-ion profile matches well with prior literature, where SEI degradation initiates thermal runaway at 110 °C, followed by exothermic reactions of intercalated Li with the electrolyte solvents over 150–250 °C [3,10]. At higher temperatures (> 250 °C), the $LiPF_6$ electrolyte salt melts and the PVDF binder reacts with Li_xC_6 by dehydrofluorination [3,13]. In comparison, the K-ion thermal runaway profile contains a large exothermic peak centered at 100 °C, as well as several minor peaks at 160 °C, 225 °C, and 325 °C. While the early peak at 100 °C initiates thermal runaway at a lower temperature than for LIB, the total heat evolved over the whole temperature range (50–450 °C) is significantly lower for K-ion (395 J g^{-1} vs. 1048 J g^{-1}) (Fig. 1c). After 195 °C, the Li-ion system generates more heat, indicating the greater stability of KIBs at higher temperatures. Depending on battery pack configuration and operation, these differences could present opportunities for safer operation. The sources of these exothermic peaks in the K-ion system cannot be determined by analogous comparison with the Li-ion profile. There are six species present in charged graphite electrodes, including K_xC_8, electrolyte, SEI, carbon black, PVDF, and possibly K metal. To determine the source of the peak at 100 °C, each of these species were individually tested to evaluate their contribution to thermal runaway.

To determine the effect of the degree of potassium intercalation, DSC profiles at various states of charge (SOC) from 0% (1.5 V) to 100% (5 mV) are shown in Fig. 2a. As the SOC increases, the total heat evolved increases from 85 J g^{-1} at 0% to 325 J g^{-1} at 100%, which is consistent with the trend for LIBs [7]. Remarkably, the primary exothermic peak shifts its center from 90 to 100 °C as the SOC increases from 25% to 100%, indicating that the full potassiation improves the thermal stability over partial potassiation. At 0% SOC, broad exotherms from 110 °C to 160 °C evolve, which could arise from SEI decomposition, as the metastable species should decompose regardless of K intercalation. This would indicate similar overall SEI thermal stability as LIBs, such that charged graphite electrode is required for thermal runaway in both systems.

Electrolyte was removed by washing the cycled electrode with dimethyl carbonate (DMC) and vacuum drying prior to DSC analysis, with the profiles shown in Fig. 2b. Regardless of the SOC, electrolyte removal results in complete loss of the peak at 100 °C, implying that intercalated K and electrolyte are required for chemical reaction. This exothermic reaction occurs in the Li-ion system, to generate SEI and heat, but from 150-250 °C [3]. Fig. S3 exhibits DSC profiles of K-ion and Li-ion electrolyte, showing that these exotherms occur only in the presence of electrolyte and intercalated graphite. In Fig. S4a, an exothermic peak occurs due to reaction of electrolyte and K metal from 140 to 170 °C, correlating with the observed peak at 160 °C, which is present only in the fully charged sample where K metal plating is most likely to occur. Fig. S4b shows the interactions of PVDF with K metal, where dehydrofluorination of PVDF to form KF likely occurs above 315 °C as seen in Fig. 1b.

To verify the proposed reaction mechanism at 100 °C, chemically synthesized KC_8 was prepared, with the structure verified by XRD in Fig. S5. This KC_8 sample does not have SEI formation, PVDF binder, or carbon black. It was found in Fig. 2c, that peaks centered at 90 °C and 140 °C were generated only by the combination of KC_8 and electrolyte. One proposed reaction, in analogy to the Li case, could be $2K + C_3H_4O_3 \rightarrow K_2CO_3 + C_2H_4$, which can be verified by additional characterization in future studies. The discrepancy in the peak center (90–100 °C) could be due to the SEI layer preventing contact of potassiated graphite with electrolyte, as Fig. 2a showed a shift with SOC and the 61% volumetric contraction could crack the SEI during depotassiation. The two peaks in Fig. 2c could correlate to phase changes, such as stage-one KC_8 to KC_{24}. To assess the reversibility of these exothermic reactions, a hermetically

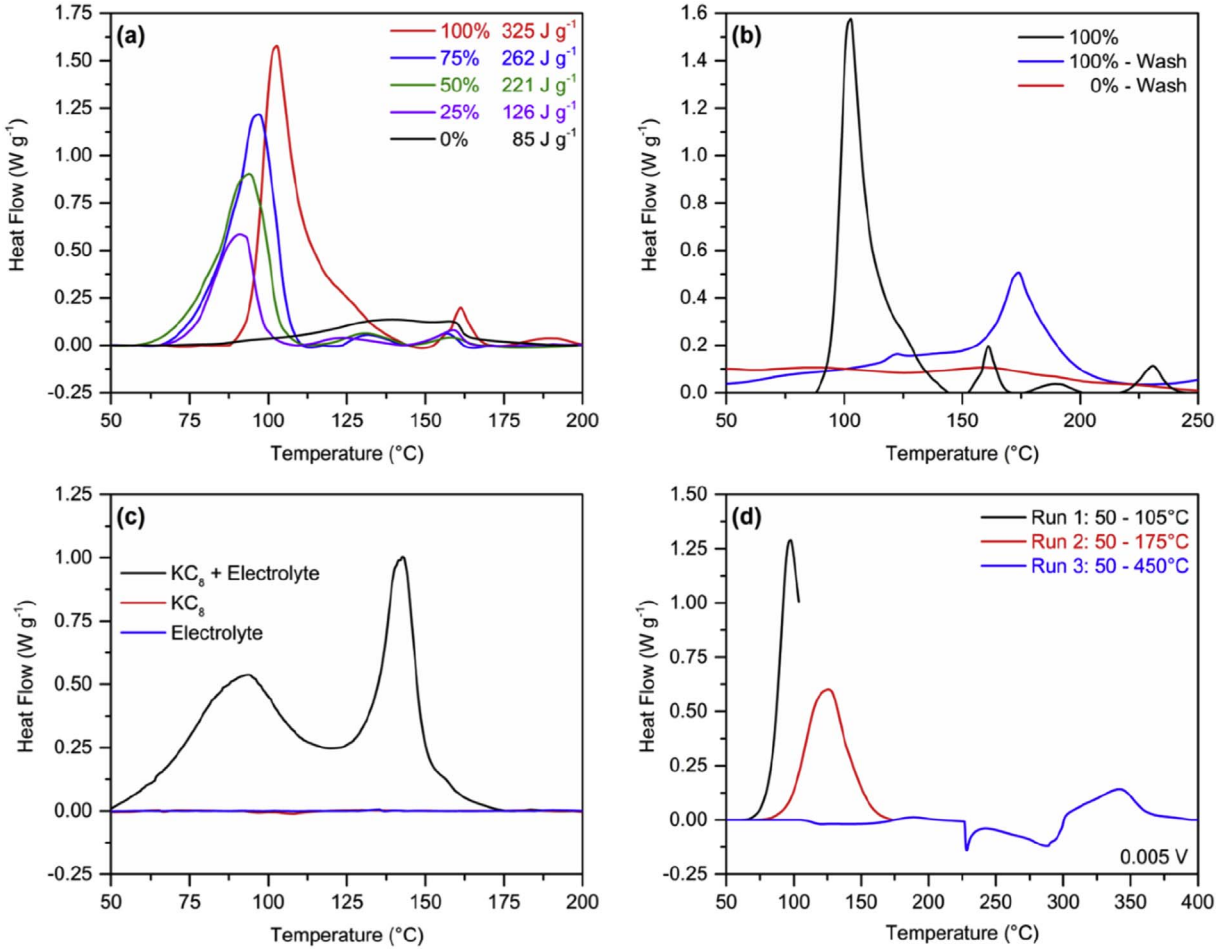


Fig. 2. (a) DSC profiles for K-ion graphite anode prepared at various states of charge from 0% (depotassiated) to 100% (potassiated). (b) DSC profiles of washed graphite electrodes to remove electrolyte. (c) DSC profiles of chemically synthesized KC_8 with electrolyte. (d) Repeated DSC analysis of K-ion graphite electrode with incrementing temperature.

sealed pan was heated three times to increasing temperatures, with the DSC profiles shown in Fig. 2d. In subsequent runs, the earlier peaks disappeared, suggesting these exothermic reactions are irreversible, similarly to the Li-ion system [3,4].

To evaluate how volumetric changes upon potassiation/depotassiation affect thermal runaway, DSC was conducted at different cycles in Fig. 3a. While thermal runaway of graphite in the Li-ion system is consistent over various cycles, KIBs decrease dramatically from cycle 1 (1170 J g^{-1}) to 10 (528 J g^{-1}) to 25 (280 J g^{-1}), due to mitigation of the peak at 100 °C. For LIB silicon anodes with 300% volume expansion, the continuous growth of SEI over time has been observed, increasing the SEI layer resistance [36]. To determine if similar phenomena occur in the K-ion graphite system, electrochemical impedance spectroscopy (EIS) spectra were collected at 200 mV (vs. K^+/K) during cycle 1, 10, and 25 with the Nyquist plot of the high frequency region shown in Fig. 3b. Fig. S6 shows Nyquist plots for the full range EIS

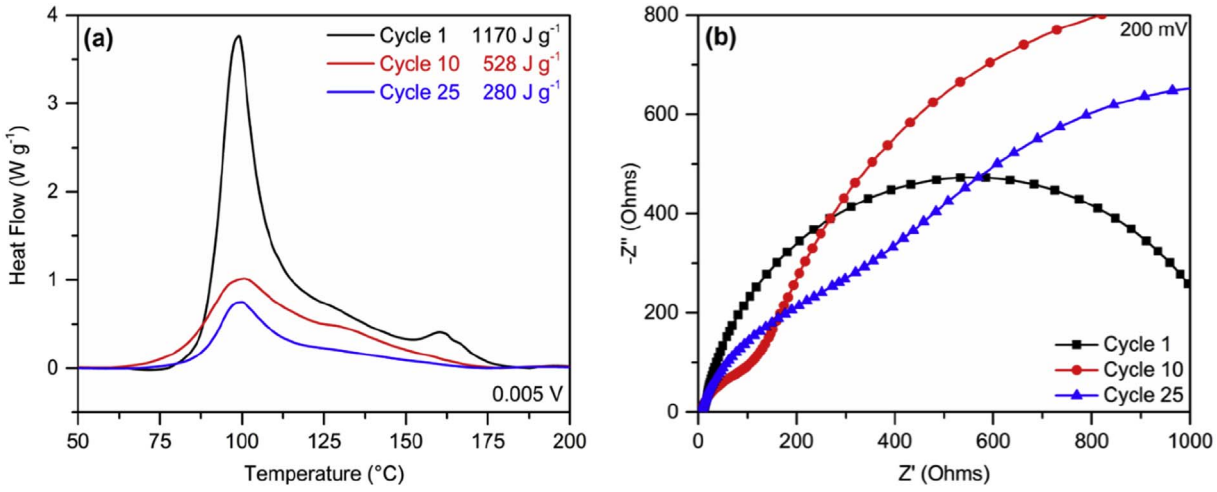


Fig. 3. (a) DSC profiles of K-ion graphite electrodes after different numbers of cycles. (b) EIS of K-ion graphite electrodes after different numbers of cycles at 200 mV vs. K^+/K.

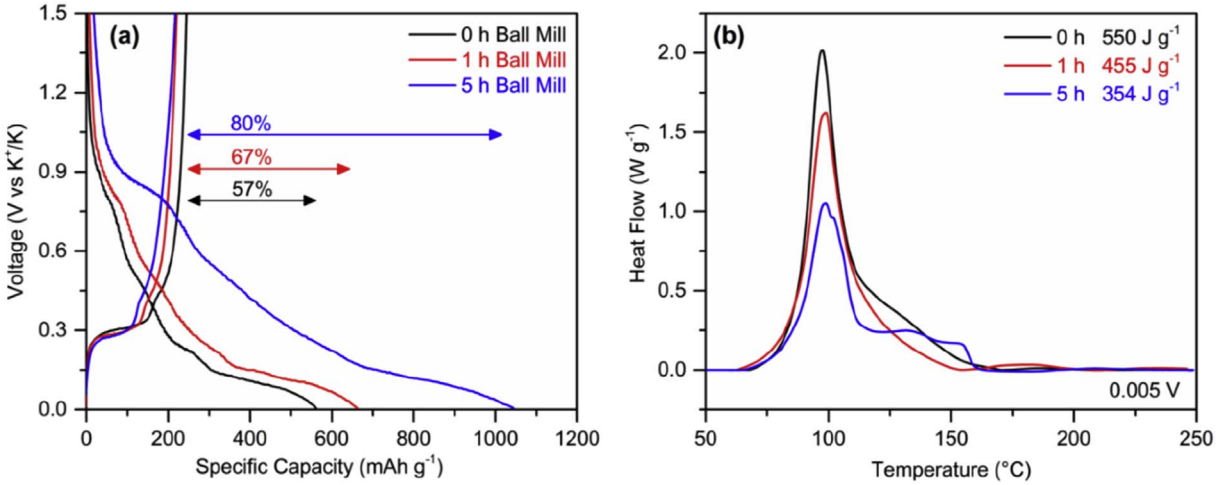


Fig. 4. (a) First cycle charge-discharge voltage profile for graphite ball milled for varying lengths of time. (b) DSC profiles for potassiated graphite electrodes after ball milling.

spectra and the corresponding equivalent circuit model. The semicircle correlating to the SEI resistance and capacitance is located at high frequencies for Li-ion graphite anodes [37]. In Fig. 3b, evolution of a distinguishable semicircle near the origin over later cycles is seen, describing the continuous growth of SEI. After fitting the equivalent circuit, R_{SEI} increases from 8.2 Ω (cycle 1) to 119.3 Ω (cycle 10) to 279.9 Ω (cycle 25). This data supports that SEI acts as a blocking mechanism for the K_xC_8 – electrolyte reaction; a similar mechanism has been proposed previously, as in LIB thermal runaway not all of the intercalated lithium is consumed, due to SEI layer growth during thermal runaway [4].

To probe the impact of SEI decomposition on thermal runaway, high surface area graphite created by ball milling was analyzed, with material properties shown in Fig. S7. Ball milling did not impact the chemical properties or crystal structuring, but only increased surface area from 2.9 $m^2 g^{-1}$ (0 h) to 43 $m^2 g^{-1}$ (1 h) to 194 $m^2 g^{-1}$ (5 h), with SEM images in Fig. S8 showing decreased particle size due to fracturing. The first cycle charge-discharge voltage profile is shown in Fig. 4a; with increasing surface area, the Coulombic efficiency decreases from 43% (0 h) to 33% (1 h) to 20% (5 h), signifying additional SEI formation. The corresponding DSC profiles are compared in Fig. 4b, where ball milling decreases heat generation from 550 J g^{-1} (0 h) to 455 J g^{-1} (1 h) to 354 J g^{-1} (5 h). In the Li-ion graphite system, higher surface area significantly augments thermal runaway, increasing the heat contribution from both SEI decomposition and Li_xC_6 – electrolyte reaction [3,4]. This unexpected result substantiates two previous claims: 1. The SEI layer blocks and prevents the K_xC_8 - electrolyte reaction. 2. K-ion SEI decomposition is comparatively insignificant in KIB thermal runaway.

Currently, little is known about SEI formation in KIBs. Wood et al. demonstrated that addition of 10 mM KPF_6 to a standard 1 M $LiPF_6$ in EC/DMC electrolyte significantly decreased the growth of dendrites on lithium metal by increasing the quantity of inorganic salts for a thinner and more conductive SEI [34]. Li^+ is solvated almost exclusively by ethylene carbonate (EC) in EC/DMC, with the following reactions resulting in SEI species of Li_2CO_3, $(CH_2OCO_2Li)_2$ oligomer, and polyethylene glycol (PEO), respectively [34].

$$EC + 2\,Li^+ + 2\,e^- \rightarrow Li_2CO_3 + H_2C = CH_2 \quad (1)$$

$$2\,EC + 2\,Li^+ + 2\,e^- \rightarrow (CH_2OCO_2Li)_2 + H_2C = CH_2 \quad (2)$$

$$nEC + 2\,Li^+ + 2\,e^- \rightarrow Li(\text{-}CH_2\text{-}CH_2\text{-}O\text{-})_nLi + n\,CO_2 \quad (3)$$

Li^+ is solvated by four EC molecules on average, whereas K^+ is solved by one, due to cationic size differences [38,39]. The Marcus reorganization energy for K^+ electro-reduction is consequently much lower than for Li^+, and the rate constant for (1) is augmented by addition of KPF_6, favoring formation of stable carbonate species relative to PEO polymer [34]. While there have not been direct studies of the SEI film formed in KIBs with carbon anodes, this study predicts that KIB SEI layer may be composed of thermally stable species, such as K_2CO_3, as opposed to metastable oligomers and PEO, whose degradation initiates thermal runaway in LIBs.

To probe the influence of binder on thermal runaway, graphite electrodes with CMCNa and Na alginate binders were analyzed. As expected, improved Coulombic efficiencies were obtained for these functionalized binders as compared to PVDF, as shown in Fig. 5a. This is due to their pre-formed SEI effect, improved coatability, and favorable mechanical properties to create a robust SEI layer [19,20]. Extended cycling is shown in Fig. S9, where CMCNa and Na alginate demonstrate superior capacity retention over 50 cycles than PVDF. The thermal runaway profiles for each binder are compared in Fig. 5b, where essentially similar heat is generated, with 373 J g^{-1} for PVDF, 481 J g^{-1} for CMCNa, and 353 J g^{-1} for Na alginate. The exothermic peak at 100 °C is broader for the functionalized binders, with the peak intensity decreasing by 35% for CMCNa and 55% for Na alginate. Instead, thermal runaway initiates earlier, at 73 °C for CMCNa and 82 °C for Na alginate, as compared to 88 °C for PVDF. While PVDF generates 86.5% of its total heat from 50-130 °C, CMCNa and Na alginate generate 55.0% and 71.8% respectively. This could be due to the preformed SEI, resulting in a composition reflective of Na-ion carbon SEI that is more vulnerable to thermal decomposition [40,41]. The decreased intensity at 100 °C correlating to the K_xC_8 – electrolyte reaction could result from improved SEI coverage and flexibility on the graphite particles throughout cycling.

Ex-situ material characterization was performed after quenching at varying temperatures during DSC to analyze the change in potassium staging during thermal runaway. The resulting XRD patterns are shown in Fig. 6a, where the broad peak centered at 19° is due to Kapton tape used to prevent sample oxidation. At 100 °C, two peaks at 30.5° and 33.3° belong to KC_{24} and KC_8 respectively [42]. At 150 °C, the (002) graphite peak at 26.5° appears, along with small peaks for KC_{36} (22.0°, 30.4°) [42]. By 250 °C, only the graphite peaks at 26.5° (002) and 54.5° (004) remain, implying that all the intercalated potassium is consumed during thermal runaway. Raman spectra in Fig. 6b confirm the presence of these intercalation stages at each quenching temperature, although some overlap between peaks complicates the analysis [42]. Stage-two KC_{24} and stage-three KC_{36} were detected previously by *ex-situ* XRD and *in-situ* Raman spectroscopy, correlating with this degradation mechanism [17,43]. In comparison to the Li-ion graphite system, analogous experiments concluded that for Li_xC_6, the change in the amount of intercalated Li was $\Delta x = 0.3$ after thermal runaway, regardless of the

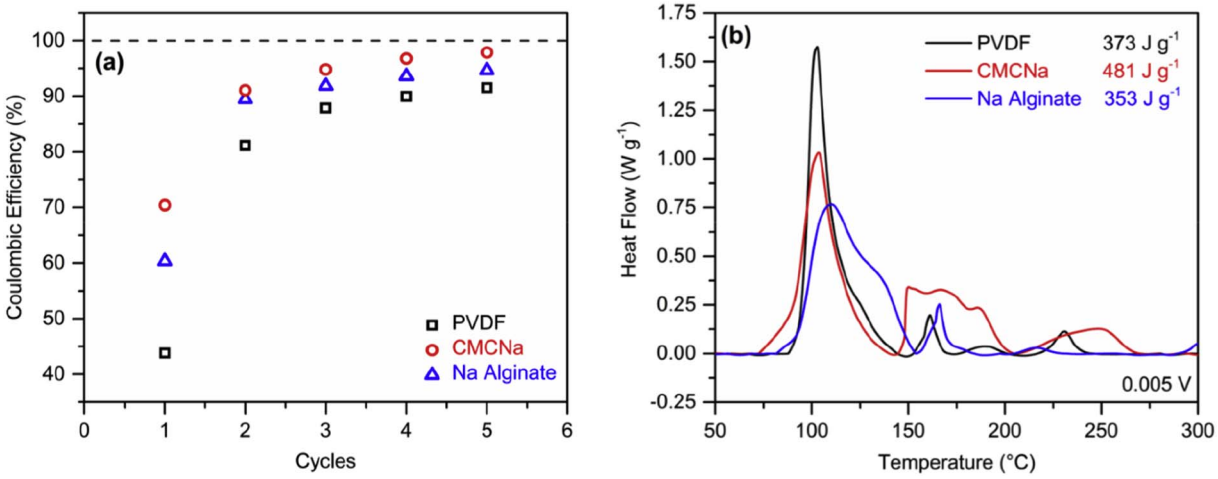


Fig. 5. (a) Coulombic efficiency for the first fives cycles of K-ion graphite electrodes using either PVDF, CMCNa, or Na alginate as binder. (b) DSC profiles of potassiated graphite electrodes prepared with different binders.

initial SOC, as SEI layer growth eventually prevents further reaction [4]. The divergence results from cracking of the SEI layer during cycling, and matches with the DSC profiles where 90% of heat is generated by 150 °C, as only graphite and KC_{36} remain.

Besides graphite, many carbons materials have been explored as K-ion anodes with exceptional cycling stability and rate capabilities. The lower density of these amorphous carbons allow them to tolerate the strain associated with insertion of bulky K^+ [21]. DSC profiles of high surface area carbon nanofiber (CNF) and Super P electrodes are shown in Fig. S10 [23]. The CNFs generated significantly lower heat of 62 J g^{-1}, as compared to 169 J g^{-1} for Super P and 324 J g^{-1} for graphite. Thermal runaway initiates at a lower temperature of 70 °C, but the low heat generation in conjunction with their promising electrochemical performance warrants further investigation [23]. The thermal stability of KIB cathodes also requires exploration, as oxygen release during breakdown of metastable Li-ion cathodes (e.g. Li_xCoO_2) initiates cell combustion during thermal runaway [6]. The matter of electrolytes also warrants further investigation, as while so far only carbonate-based electrolytes (e.g. EC, DEC) have been utilized in non-aqueous KIBs, alternative systems and electrolyte additives could possibly provide benefits of electrochemical performance and safety [44].

4. Conclusion

Thermal runaway of graphite anodes for KIBs was investigated for the first time utilizing DSC analysis. The KIB graphite anode initiates thermal runaway at 100 °C, due to exothermic reaction of KC_8 – electrolyte, but generates only 395 J g^{-1} versus 1048 J g^{-1} for Li-ion from 50-450 °C. A strong dependence on SOC, cycle number, and carbon material properties was found, due to the large volumetric expansion of graphite upon potassiation, causing SEI layer cracking and growth over time. Functionalized binders (CMCNa and Na alginate) mitigate the exothermic peak at 100 °C by preventing K_xC_8 – electrolyte contact through improved SEI layer coverage, but decrease the inherent thermal stability of K-ion SEI. *Ex-situ* XRD and Raman spectroscopy verified the complete consumption of intercalated K, explaining the strong intensity of the exotherm at 100 °C. These findings suggest future strategies to improve KIB safety, where establishment of a robust SEI layer with complete graphite particle coverage can mitigate this initiating reaction. The significantly decreased heat generation and promise of non-graphitic carbon anodes also warrant further investigation into the safety of K-ion batteries for rechargeable energy storage. In summary, potassium battery graphitic anodes are prone to thermal runaway at lower temperature but overall heat generation is less as compared to conventional lithium ion battery anodes.

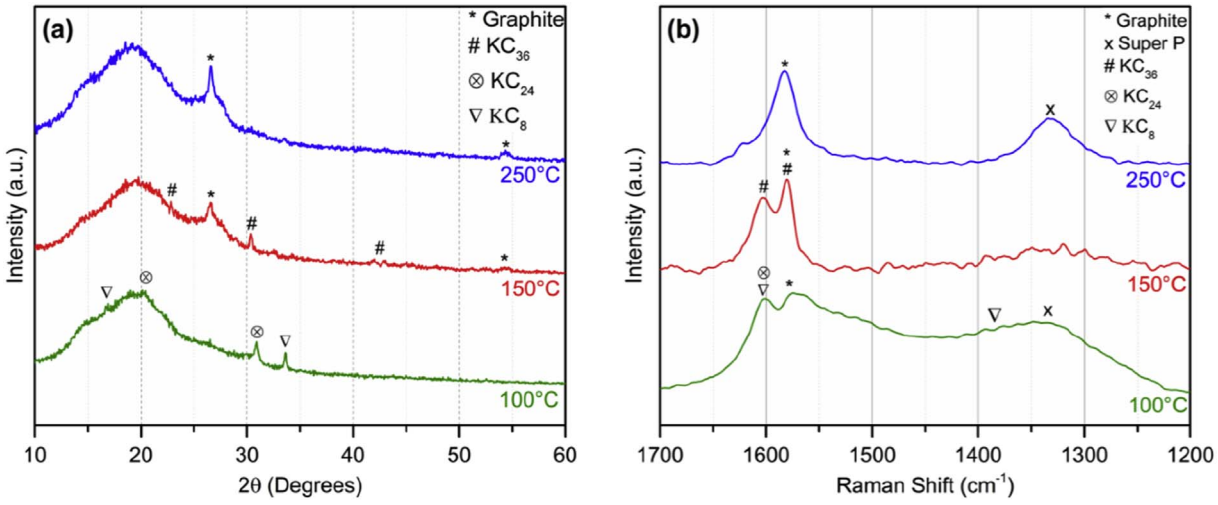


Fig. 6. (a) XRD patterns of potassiated graphite quenched at 100 °C, 150 °C, or 250 °C. (b) Raman spectra of potassiated graphite quenched at 100 °C, 150 °C, or 250 °C.

Acknowledgments

V.P. thanks Purdue University and its Davidson School of Chemical Engineering for the generous start-up funding. The Slayter Discretionary Fund (A.V.) was used to purchase chemical and laboratory supplies. VP thanks the Office of Naval Research for supporting this project under Naval Enterprise Partnership Teaming with Universities for National Excellence (NEPTUNE Phase I and II) at Purdue Center for Power and Energy Research provided under grant number N00014-15-1-2833.

Appendix A. Supplementary data

Supplementary data related to this article can be found at http://dx.doi.org/10.1016/j.jpowsour.2017.11.065.

References

[1] T.M. Bandhauer, S. Garimella, T.F. Fuller, A critical review of thermal issues in lithium-ion batteries, J. Electrochem. Soc. 158 (2011) R1–R25.
[2] X. Feng, M. Ouyang, X. Liu, L. Lu, Y. Xia, X. He, Thermal runaway mechanism of lithium ion battery for electric vehicles: a review, Energy Storage Mater 10 (2018) 246–267.
[3] A. Du Pasquier, F. Disma, T. Bowmer, A.S. Gozdz, G. Amatucci, J. Tarascon, Differential scanning calorimetry study of the reactivity of carbon anodes in plastic Li-Ion batteries, J. Electrochem. Soc. 145 (1998) 472–477.
[4] M.N. Richard, J.R. Dahn, Accelerating rate calorimetry study on the thermal stability of lithium intercalated graphite in electrolyte I. Experimental, J. Electrochem. Soc. 146 (1999) 2068–2077.
[5] Y. Fu, S. Lu, K. Li, C. Liu, X. Cheng, H. Zhang, An experimental study on burning behaviors of 18650 lithium ion batteries using a cone calorimeter, J. Power Sources 273 (2015) 216–222.
[6] J. Dahn, E. Fuller, M. Obrovac, U. Vonsacken, Thermal stability of LixCoO2, LixNiO2 and λ-MnO2 and consequences for the safety of Li-ion cells, Solid State Ionics 69 (1994) 265–270.
[7] Q. Wang, J. Sun, X. Yao, C. Chen, Thermal behavior of lithiated graphite with electrolyte in lithium-ion batteries, J. Electrochem. Soc. 153 (2006) A329–A333.
[8] O.S. Mendoza-Hernandez, H. Ishikawa, Y. Nishikawa, Y. Maruyama, M. Umeda, Cathode material comparison of thermal runaway behavior of Li-ion cells at different state of charges including over charge, J. Power Sources 280 (2015) 499–504.
[9] Q. Wang, P. Ping, X. Zhao, G. Chu, J. Sun, C. Chen, Thermal runaway caused fire and explosion of lithium ion battery, J. Power Sources 208 (2012) 210–224.
[10] G. Gachot, S. Grugeon, G.G. Eshetu, D. Mathiron, P. Ribière, M. Armand, et al., Thermal behaviour of the lithiated-graphite/electrolyte interface through GC/MS analysis, Electrochim. Acta 83 (2012) 402–409.
[11] H.H. Lee, C.C. Wan, Y.Y. Wang, Thermal stability of the solid electrolyte interface on carbon electrodes of lithium batteries, J. Electrochem. Soc. 151 (2004) A542–A547.
[12] L. Ma, J. Xia, X. Xia, J.R. Dahn, The impact of vinylene carbonate, fluoroethylene carbonate and vinyl ethylene carbonate electrolyte additives on electrode/electrolyte reactivity studied using accelerating rate calorimetry, J. Electrochem. Soc. 161 (2014) A1495–A1498.
[13] C. Forestier, S. Grugeon, C. Davoisne, A. Lecocq, G. Marlair, M. Armand, et al., Graphite electrode thermal behavior and solid electrolyte interphase investigations: role of state-of-the-art binders, carbonate additives and lithium bis(fluorosulfonyl) imide salt, J. Power Sources 330 (2016) 186–194.
[14] A. Eftekhari, Z. Jian, X. Ji, Potassium secondary batteries, ACS Appl. Mater. Interfaces 9 (2017) 4404–4419.
[15] J.C. Pramudita, D. Sehrawat, D. Goonetilleke, N. Sharma, An initial review of the status of electrode materials for potassium-ion batteries, Adv. Energy Mater (2017) 1602911.
[16] N. Yabuuchi, K. Kubota, M. Dahbi, S. Komaba, Research development on sodium-ion batteries, Chem. Rev. 114 (2014) 11636–11682.
[17] Z. Jian, W. Luo, X. Ji, Carbon electrodes for K-Ion batteries, J. Am. Chem. Soc. 137 (2015) 11566–11569.
[18] W. Luo, J. Wan, B. Ozdemir, W. Bao, Y. Chen, J. Dai, et al., Potassium ion batteries with graphitic materials, Nano Lett. 15 (2015) 7671–7677.
[19] S. Komaba, T. Hasegawa, M. Dahbi, K. Kubota, Potassium intercalation into graphite to realize high-voltage/high-power potassium-ion batteries and potassium-ion capacitors, Electrochem. Commun. 60 (2015) 172–175.
[20] J. Zhao, X. Zou, Y. Zhu, Y. Xu, C. Wang, Electrochemical intercalation of potassium into graphite, Adv. Funct. Mater 26 (2016) 8103–8110.
[21] Z. Jian, Z. Xing, C. Bommier, Z. Li, X. Ji, Hard carbon microspheres: potassium-ion anode versus sodium-ion anode, adv, Energy Mater 6 (2015) 1501874.
[22] Y. Liu, F. Fan, J. Wang, Y. Liu, H. Chen, K. Jungjohann, et al., In situ TEM study of electrochemical sodiation and potassiation of carbon nanofibers, Nano Lett. 14 (2014) 3445–3452.
[23] R.A. Adams, J.-M. Syu, Y. Zhao, C.-T. Lo, A. Varma, V.G. Pol, Flexible, binder-free, N- and O- rich carbon nanofiber anodes for long cycle life K-ion batteries, ACS Appl. Mater. Interfaces 9 (2017) 17872–17881.
[24] Z. Ju, S. Zhang, Z. Xing, Q.-C. Zhuang, Y.-H. Qiang, Y. Qian, Directly synthesis few-layer F-doped graphene foam and its lithium/potassium storage properties, ACS Appl. Mater. Interfaces 8 (2016) 20682–20690.
[25] K. Share, A.P. Cohn, R. Carter, B. Rogers, C.L. Pint, Role of nitrogen-doped graphene for improved high-capacity potassium ion battery anodes, ACS Nano 10 (2016) 9738–9744.
[26] Z. Xing, Y. Qi, Z. Jian, X. Ji, Polynanocrystalline graphite: a new carbon anode with superior cycling performance for K-Ion batteries, ACS Appl. Mater. Interfaces 9 (2017) 4343–4351.
[27] Y. Li, R.A. Adams, A. Arora, V.G. Pol, A.M. Levine, R.J. Lee, et al., Sustainable potassium-ion battery anodes derived from waste-tire rubber, J. Electrochem. Soc. 164 (2017) A1234–A1238.
[28] C. Vaalma, G.A. Giffin, D. Buchholz, S. Passerini, Non-aqueous K-Ion battery based on layered K0.3MnO2 and hard carbon/carbon black, J. Electrochem. Soc. 163 (2016) A1295–A1299.
[29] X. Wang, X. Xu, C. Niu, J. Meng, M. Huang, X. Liu, et al., Earth abundant Fe/Mn-Based layered oxide interconnected nanowires for advanced K-Ion full batteries, Nano Lett. 7 (2017) 544–550.
[30] H. Kim, J.C. Kim, S.-H. Bo, T. Shi, D.-H. Kwon, G. Ceder, K-ion batteries based on a P2-Type K0.6CoO2 cathode, Adv. Energy Mater (2017) 1700098.
[31] K. Chihara, A. Katogi, K. Kubota, S. Komaba, KVPO4F and KVOPO4 toward 4 volt-class potassium-ion batteries, Chem. Commun. 53 (2017) 5208–5211.
[32] M. Moshkovich, Y. Gofer, D. Aurbach, Investigation of the electrochemical windows of aprotic alkali metal (Li, Na, K) salt solutions, J. Electrochem. Soc. 148 (2001) E155–E167.
[33] Q.C. Zhuang, J. Li, L.L. Tian, Potassium carbonate as film forming electrolyte additive for lithium-ion batteries, J. Power Sources 222 (2013) 177–183.
[34] S.M. Wood, C.H. Pham, R. Rodriguez, S.S. Nathan, A.D. Dolocan, H. Celio, et al., K + reduces lithium dendrite growth by forming a thin, less-resistive solid electrolyte interphase, ACS Energy Lett. 1 (2016) 414–419.
[35] M. Ouyang, Z. Chu, L. Lu, J. Li, X. Han, X. Feng, et al., Low temperature aging mechanism identification and lithium deposition in a large format lithium iron phosphate battery for different charge profiles, J. Power Sources 286 (2015) 309–320.
[36] M. Nie, D. Chalasani, D.P. Abraham, Y. Chen, A. Bose, B.L. Lucht, Lithium ion battery graphite solid electrolyte interphase revealed by microscopy and spectroscopy, J. Phys. Chem. C 117 (2013) 13403–13412.
[37] S.S. Zhang, K. Xu, T.R. Jow, EIS study on the formation of solid electrolyte interface in Li-ion battery, Electrochim. Acta 51 (2006) 1636–1640.
[38] I. Skarmoutsos, V. Ponnuchamy, V. Vetere, S. Mossa, Li+ solvation in pure, binary, and ternary mixtures of organic carbonate electrolytes, J. Phys. Chem. C 119 (2015) 4502–4515.
[39] H. Wang, M. Yoshio, KPF6 dissolved in propylene carbonate as an electrolyte for activated carbon/graphite capacitors, J. Power Sources 195 (2010) 1263–1265.
[40] M. Dahbi, N. Yabuuchi, K. Kubota, K. Tokiwa, S. Komaba, Negative electrodes for Na-ion batteries, Phys. Chem. Chem. Phys. 16 (2014) 15007–15028.
[41] S.J. An, J. Li, C. Daniel, D. Mohanty, S. Nagpure, D.L. Wood, The state of understanding of the lithium-ion-battery graphite solid electrolyte interphase (SEI) and its relationship to formation cycling, Carbon 105 (2016) 52–76.
[42] J. Purewal, Hydrogen Adsorption by Alkali Metal Graphite Intercalation Compounds, (2010).
[43] K. Share, A.P. Cohn, R.E. Carter, C.L. Pint, Mechanism of potassium ion intercalation staging in few layered graphene from in situ Raman spectroscopy, Nanoscale 8 (2016) 16435–16439.
[44] P.G. Balakrishnan, R. Ramesn, T. Prem Kumar, Safety Mechanisms in lithium-ion batteries, J. Power Sources 155 (2006) 401–414.